



# VASIM: an automated tool for the quantification of carotid atherosclerosis by computed tomography angiography

Florentino Luciano Caetano dos Santos<sup>1,4,5</sup> · Marcin Kolasa<sup>4</sup> · Mitsugu Terada<sup>2</sup> · Juha Salenius<sup>3</sup> · Hannu Eskola<sup>1,4</sup> · Michelangelo Paci<sup>1</sup>

Received: 24 September 2018 / Accepted: 28 January 2019 / Published online: 28 February 2019  
© Springer Nature B.V. 2019

## Abstract

The diagnostic imaging techniques currently used to evaluate the arterial atherosclerosis hinge on the manual marking and calculation of the stenosis degree. However, the manual assessment is highly dependent on the operator and characterized by low replicability. The study aimed to develop a fully-automated tool for the segmentation and analysis of atherosclerosis in the extracranial carotid arteries. The dataset consisted of 59 randomly-chosen individuals who had undergone head-and-neck computed tomography angiography (CTA), at the Tampere University Hospital, Tampere, Finland. The analysis algorithm was mainly based on the detection of carotid arteries, delineation of the vascular wall, and extraction of the atherosclerotic plaque. To improve the vascular detection rate, the model-based and volume-wide analytical approaches were deployed. A new fully-automated vascular imaging (VASIM) software tool was developed. For stenosis over 50%, the success rate was 83% for the detection and segmentation. Specificity and sensitivity of the algorithm were 25% and 83%, respectively. The overall accuracy was 71%. The VASIM tool is the first published approach for the fully-automated analysis of atherosclerosis in extracranial carotid arteries. The tool provides new outputs, which may help with the quantitative and qualitative, clinical evaluation of the atherosclerosis burden and evolution. The findings from this study provide a basis for the further development of automated atherosclerosis diagnosis and plaque analysis with CTA.

**Keywords** Carotid atherosclerosis · Angiography · Computer-assisted image analysis · Computer-assisted diagnosis

## Abbreviations

CCA	Common carotid artery	ECA	External carotid artery
CT	Computed tomography	HU	Hounsfield unit
CTA	Computed tomography angiography	ICA	Internal carotid artery
CVAs	Cerebrovascular accidents	MRI	Magnetic resonance imaging
CVDs	Cardiovascular diseases	NASCET	North American Symptomatic Carotid Endarterectomy Trial
		SD	Standard deviation
		TAYS	Tampere University Hospital
		VASIM	Vascular imaging

✉ Florentino Luciano Caetano dos Santos  
florentino.l.c.santos@ieee.org

<sup>1</sup> BioMediTech, Faculty of Medicine and Health Technology, Tampere University, SM312, Korkeakoulunkatu 3, 33720 Tampere, Finland

<sup>2</sup> Department of Applied Physics, Faculty of Science, Fukuoka University, Fukuoka, Japan

<sup>3</sup> Division of Vascular Surgery, Department of Surgery, Tampere University Hospital and Medical School, Tampere, Finland

<sup>4</sup> Department of Radiology, Medical Imaging Center, Tampere University Hospital, Tampere, Finland

<sup>5</sup> BioMediTech, Faculty of Medicine and Health Technology, Tampere University, P.O. Box 692, Tampere 33014, Finland

## Introduction

Cardiovascular diseases (CVDs) are the leading cause of death worldwide. According to the World Health Organization, in 2012, 37% of premature deaths were caused by CVDs. This translated to 17.5 million deaths, of which 6.7 million were due to cerebrovascular accidents (CVAs) [1, 2]. Majority of CVAs are ischemic strokes, caused mainly by atherosclerosis.

Existing research recognizes the critical role of early diagnosis and treatment of atherosclerosis in CVDs mortality prevention [3]. A considerable amount of literature has been published on diagnostic accuracy that has been improved by new imaging techniques, image processing, and image analysis methods [4, 5].

Computed tomography angiography (CTA), is a common modality for imaging the carotid arteries. Currently, evaluating atherosclerotic lesions is based on the degree of maximal luminal stenosis, and the composition and morphology of the plaque [6–8]. However, assessment of these parameters is performed manually.

The manual assessment has several major limitations, including operator dependency, long analysis time, questionable analysis dependability and repeatability [9]. It has been reported that the inter- and intra-operator variability (coefficients of variation) for plaque area measurements were 19% and 8%, respectively [10]. Despite these major limitations, manual stenosis level measurement, e.g., using the North American Symptomatic Carotid Endarterectomy Trial (NASCET) [11] criterion, remains the main accepted metric for determining the urgency of prevention and treatment. There remains a need for a fully-automated method of carotid artery analysis, providing both satisfactory running time and reliability.

The previous research by the authors has established: (i) the initial semi-automated segmentation of the carotid arteries based on manual seeding [6], (ii) the fully automated detection of the carotid arteries allowing to avoid manual seeding [9], and (iii) the automated carotid walls contour segmentation [12].

The main aim of this study was to develop a fully-automated tool for atherosclerosis segmentation and analysis in the carotid arteries. This paper describes the design and implementation of a new vascular imaging (VASIM) software tool, which is a fully-automated and structured integration of all methods previously established by the authors.

## Materials and methods

### Study population

The source population for this study were patients obtained from the Tampere University Hospital (TAYS), Tampere, Finland, between the January 1st, 2008 and December 31st, 2015. The study population was recruited retrospectively from the TAYS database. All patients were selected randomly.

Inclusion criteria were defined a priori as follows: a patient with at least one head-and-neck CTA scan (i.e., aorta arch to skull apex). The exclusion criteria were defined as: patients with CT scan only (without CTA); patients with

incomplete medical records, i.e., without sufficient data on CTA technical information.

From the TAYS patient's population, all were randomly selected and the final study population consisted of 59 patients (N = 59): 34 men (58%) and 25 women (42%). The mean age was 64 years (standard deviation (SD) 14), ranging from 12 to 83 years.

Head-and-neck CTA scans of all 59 individuals were retrospectively reassessed, and the stenosis levels were manually calculated according to the NASCET criteria. Subsequently, based on the level of stenosis, individuals were included in one of the two groups—cases or controls. Cases were defined as individual carotids with stenosis  $\geq 50\%$ . Controls were all individual carotids with stenosis  $< 50\%$ .

The study was approved by the Ethical Committee of Pirkanmaa Hospital District, Tampere, Finland (decision number R07210).

### Imaging

CTAs were performed using helical, 64-slice, multidetector CT scanners; either a General Electric LightSpeed (slice thickness 1.25 mm; increment 0.5–0.7 mm; pixel size 0.6–0.7 mm; 120 kVp; 130–327 mAs) or a Philips Brilliance CT 64-slice (slice thickness 1 mm; increment 0.5 mm; pixel size 0.42–0.49 mm; 120 kVp; 178–243 mAs). All of the images were exported in DICOM® standard, as a 512 × 512 matrix.

To improve carotid artery contrast, one of the following CTA contrast media was used: Iomeron® 350 mg/ml, Omnipaque® (350 mg/ml; General Electric), and Xenetix® (350 mg/ml; Guerbet). They were administered intravenously (ulnar or palmar vein), in accordance with the manufacturers' instructions.

### Image analysis

VASIM's image analysis algorithm was divided into five consecutive stages: (i) loading of the patient's stack; (ii) carotid arteries detection, subdivided into airways segmentation and carotid segmentation; (iii) vascular wall delineation; (iv) atherosclerotic plaque extraction; (v) metrics, 2D tissue masks, 3D model calculation, and rendering. Figure 1 depicts the general analysis diagram followed by VASIM.

### Automatic detection of carotid arteries

The detection methodology was explained on an example of the Patient 3 (75 years-old male). This patient had previously suffered a transient ischemic attack, and had arterial hypertension and hyperlipidemia history. Carotid arteries component evaluation detected a plaque of mixed nature

(fibrosis, lipid pool, and calcification) located in the right internal carotid artery (ICA), causing a 75% stenosis.

**Airways segmentation** As in the previous study of the authors [9], the first step of the carotid arteries detection was creating an anatomical landmark, based on the upper respiratory tract (i.e., above the sternal angle) (Fig. 1a.1). The image analysis was restricted to the level of the auditory tube opening, which approximates the carotid canal level.

Airways provided the axis for a cylindrical volume-of-interest. This enabled the detection of vascular trees rather than slice-wise circular structures. To create the airways models, a hard threshold of  $-500$  Hounsfield units was applied. To exclude the air surrounding a patient, objects connected to the volume borders were discarded. Figure 2 shows an example of airways model for the Patient 3.

Additionally, the airways landmark enabled normalizing the dataset by the patient's body size.

**Automatic segmentation of the carotid vessel** During the automatic analysis of CTA neck cross-sections, several structures can be misclassified as the carotid arteries, e.g., feeding tubes, needles, and jugular veins.

In the previous study [9], the algorithm identified carotid arteries between two anatomical structures: brachiocephalic artery bifurcation and circle of Willis. However, that method was dependent on manual seeding and parameterization. Therefore, here, a new method based on a fully-automated volume-of-interest analysis is presented.

In the first stage, a tilted cylinder (radius of 5 cm) was created around the airways, on the section between the most proximal and distant CTA slices. Subsequently, the resultant model was cleaned from lower attenuation tissues (e.g., lipid pools), using MATLAB's native *isovalue* function. The airways divided objects into the right and left side. The division enabled estimation of their interconnectivity. Single, uncompromised arteries were accepted as the final model. In the case of completely occluded arteries, their continuity was assessed distantly to the occlusion (Fig. 1a.2).

Sporadically, after thresholding, the algorithm presented objects that crossed the sagittal plane of the airways. Examples of such objects were the mandible and hyoid bone. The contrast between arteries and objects mentioned above may be insufficient to distinguish these structures. Figure 3 presents an example of a horizontal object (thyroid cartilage) connecting both arterial trees into a single volume.

The separation of the carotids and other objects was divided into the following steps: (i) volume skeletonization [13], (ii) skeleton nodes (branching points) location and removal, (iii) vertical degree evaluation of each resultant object, (iv) non-vertical removal, and (v) reconstruction of arterial trees using the acquired volume skeleton and the original 3D model. The bounding box dimension of each

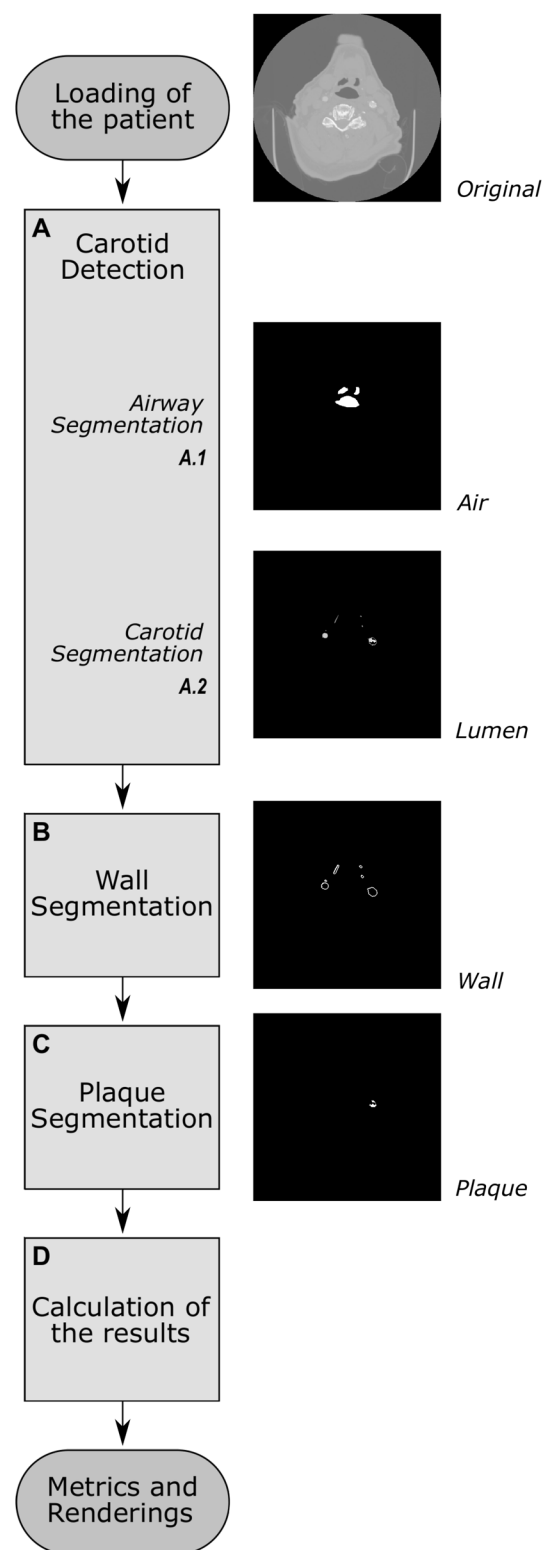


Fig. 1 VASIM protocol diagram

object was used to determine the vertical degree. Every object with a  $z/x$ -axis or  $z/y$ -axis ratio  $< 1.5$  was discarded from the volume.

**Fig. 2** Segmented airways for Patient 3 (seen from the anterior plane)



The current methodology and handling of possible hindrances resulted in two carotid models. Each artery skeleton was recalculated and used to define the carotid area

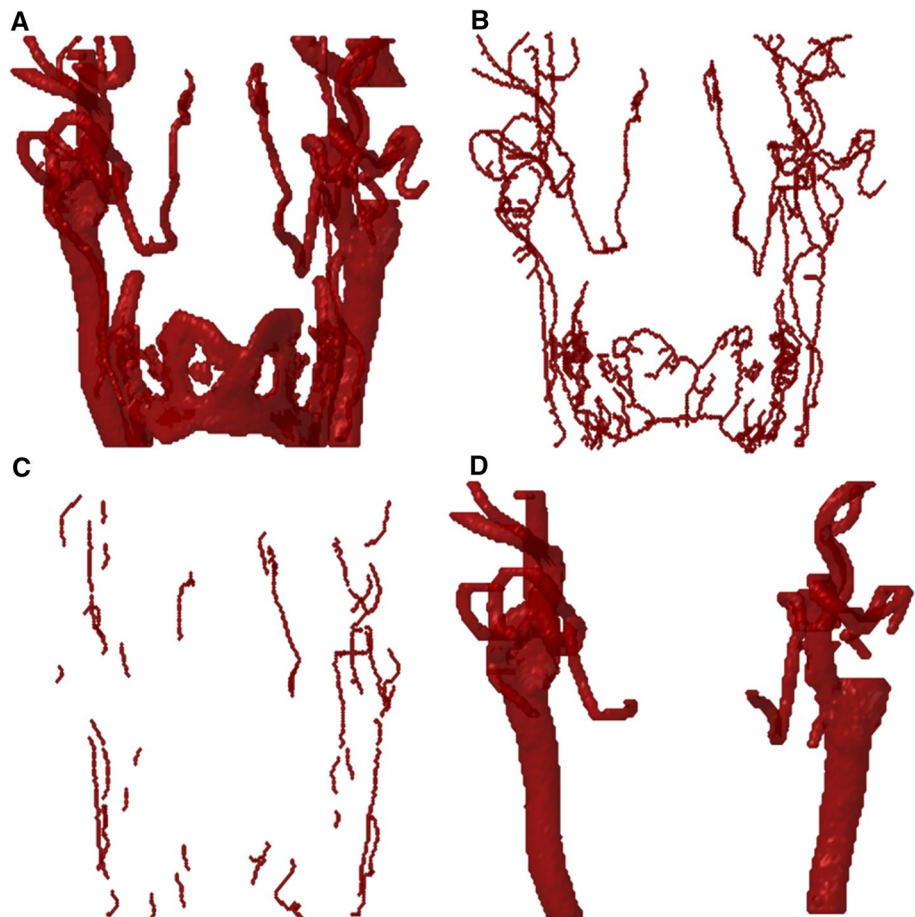
perpendicularly to the vascular curvature. This prevented incorrect cross-sections, e.g., in horizontal branches of the ICA.

To ensure contradistinction between the common carotid artery (CCA), ICA, and external carotid artery (ECA), the algorithm initially detected the CCA bifurcation. The bifurcation location was defined as the most proximal cross-section where the number of objects increased from one to two, and the distance between their centroids was smaller than  $< 1$  cm. The latter rule prevented potential errors caused by loops in the distant segment of the artery. The separation between ECA and ICA was conducted using the vertical degree threshold as previously used in the separation between arterial tree and surrounding objects.

### Segmentation of the outer carotid wall

To calculate the vascular wall thickness the lumen and carotid wall boundaries were delimited. A method based on morphological operators and edge enhancers/detectors was used (Fig. 1b) to define the boundary of the carotid wall. This method was described in detail in a previous study by the group [12].

**Fig. 3** Example of thyroid region spillage (Patient 3). **a** Two carotids visible with a horizontal structure joining both arteries into the same volume. **b** Model's skeleton. **c** Vertical elements of the skeleton. **d** Resulting model after connecting vertical objects' centroids in the original model





## Plaque volume extraction

For segmenting the carotid plaque and assessing its morphology, a new method was developed. This was accomplished similarly to the airways segmentation. However, the threshold value was defined using the histogram of the maximum-intensity projections on the three axes. In each maximum-intensity projection, a threshold value based on the Otsu method [14] was calculated. Subsequently, the three values were averaged and applied to the 3D volume. The automatic threshold was deployed to address high variability in patient atherosclerosis level, which demanded a higher adaptability from the method. This considerably reduced the time required for plaque segmentation compared with the previously deployed algorithm [13] (Fig. 1c). Following this processing, a 3D rendering of the three major components of the carotid was produced. It presented lumen, the vascular wall, and any possible atherosclerotic plaque. Example of such a presentation is shown in Fig. 4. The plaques were poorly visualized as they are always located between the lumen and the outer vascular wall. Therefore, they were modeled in Fig. 4c with the open lumen path.

## Metrics evaluated

The current protocol allows side-wise extraction of the following metrics: the minimum lumen area in the region of interest; the maximum area percentage occupied by the arterial wall in a slice; the maximum area percentage occupied by the plaque; and the maximum stenosis of the carotid artery calculated by the algorithm (Fig. 1d). Moreover, location-specific stenosis can be calculated for the CCA, ICA, and ECA. In our study, the region of interest was comprised of the CCA and ICA models, which were used for stenosis calculation. All of the stenosis values are calculated according to the NASCET criteria, i.e., one minus the minimum lumen area in the region of interest divided by the assumed healthy lumen area in the region of interest. Prior to the NASCET stenosis calculation, the equivalent diameter of the perpendicular-corrected section of the vessel model was calculated.

Following the development of the automated stenosis assessment with the VASIM methodology, the data on manually calculated stenosis values were obtained from medical records. The manual assessment was performed by an experienced radiologist beforehand, which ensured blinding to the VASIM results. Subsequently, the absolute difference between the manually and automatically calculated stenosis values was computed. Only arteries with both manually- and automatically-determined stenosis percentages were taken into consideration for the statistical calculations.

The classification as a case or control (binary classification test) was based on the manually assessed level of

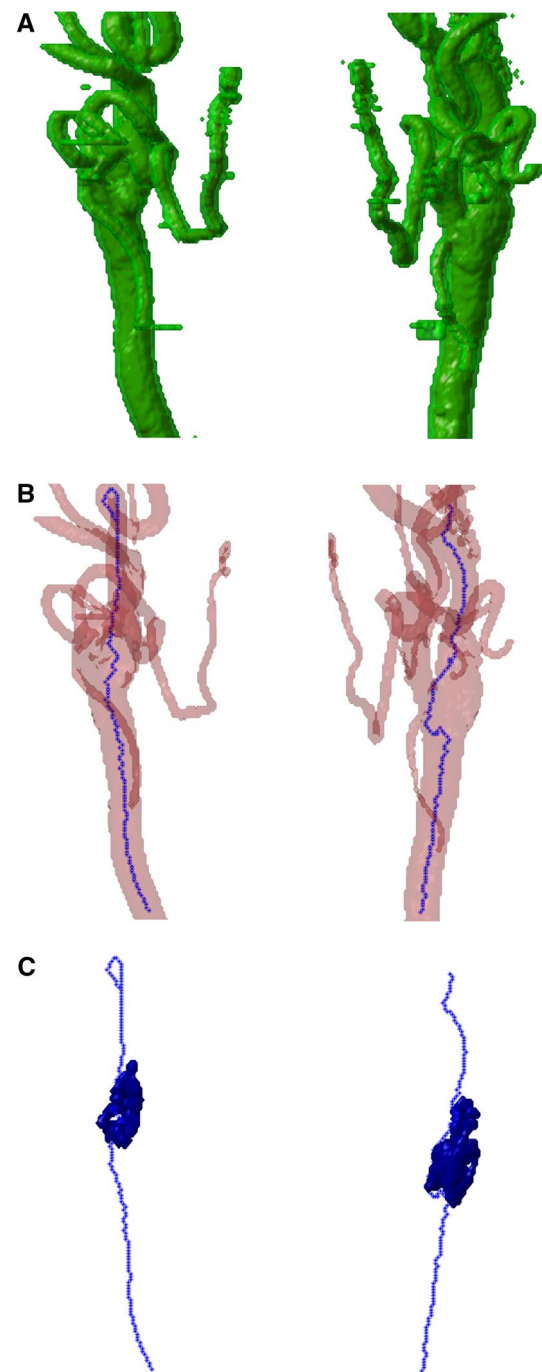


**Fig. 4** Full rendering of the carotid structures (Patient 3). **a** Carotid walls (green). **b** Overlay of the semi-transparent lumen (red) and carotid open pathway (dotted blue line). **c** Carotid open lumen pathway (dotted blue line) and calcified plaque elements (blue volumes)

stenosis. According to the NASCET, the demonstrated, conclusive benefit for carotid endarterectomy is observed in patients with symptomatic 70–99% ICA stenosis [11]. Notwithstanding, in this study, the cut-off point between cases and controls was stenosis of 50%. The justification for this cut-off point was the fact, that according to the European

Association of Vascular Surgery endarterectomy is more appropriate for symptomatic 50–99% stenosis patients, and for asymptomatic 70–99% stenosis patients [15].

Furthermore, sensitivity, specificity, and accuracy of our method were assessed. The VASIM performance was evaluated based on the tissue segmentation success rate, variation between manually and automatically calculated stenosis values, and the total analysis time. The Pearson's coefficient was used for hypothesis test evaluation. The success of the segmentation was determined visually by the operator. The assessment was based on volume comparison and segmentation masks with the image stack for the verification of the correct tissue detection and segmentation (airway, lumen, wall, and plaque).

The atherosclerotic plaque accuracy evaluation based on the comparison with histopathology was not performed. It was previously demonstrated, that both endarterectomy procedure and pre-histopathological preparation affect the plaque's morphology. Hence, the comparison between the in-vivo CTA plaque and the ex-vivo sample is impossible [16].

Finally, a user-friendly and intuitive graphical interface was developed.

VASIM and its underlying algorithms were developed and tested on a Lenovo workstation (Lenovo W541, Windows 7 Enterprise, 64 bits, 4 2.80 GHz, 32.0 GB RAM) equipped with the MATLAB (version R2017a, Image Processing Toolbox version 10.0, Signal Processing Toolbox version 7.4, and Statistical Analysis and Machine Learning Toolbox version 11.1).

## Results

In this study, a new VASIM software tool was designed, developed, and used to assess atherosclerosis in the CCA and the cervical segment of the ICA.

The overall tissue segmentation (lumen, wall, and plaque) success rate was 83%, equivalent to 49 out of 59 correctly identified carotids. The average absolute difference between the manual and automated stenosis calculations was 37% (95% confidence interval 29–46%) (Tables 1, 2). The *p*-value for the automated and manual analysis was 0.2976.

Forty-two atherosclerotic plaques were identified in the study population (Table 1). Forty of them were located in the ICA, and two in the CCA. Based on the morphology, the plaques mentioned above can be classified into the following categories: 13 of mixed nature, 23 calcified, two ulcerated, two soft tissue, and two irregular.

VASIM's overall accuracy was 71%. The average time for the whole procedure (loading of patient's volume, airways segmentation, carotid detection and segmentation, vascular wall and plaque segmentation, quantitative results, 3D

modeling, and saving of results) was 1381 s. The average analysis time was 1.62 s per slice. The number of slices was different for each patient. Table 2 presents the summary statistics for the stenosis metrics.

The detected carotid arteries were subsequently classified into two groups, i.e., stenosis < 50% and  $\geq$  50% (Table 3). The 32 manually-detected  $\geq$  50% stenoses were compared with the automated analysis performed with the VASIM.

In cases of stenosis  $\geq$  50%, the sensitivity and specificity were 83% and 25%, respectively. The confusion matrix used in the metrics calculation is presented in Table 4.

The VASIM interface provided three main functions (Fig. 5a): patient image stack loading, analyzing the data, and creating a 3D model. The facultative "Model" function allowed to obtain a 3D model, based on current window and level values. In Fig. 5a, the "Analyze" button is hidden as the analysis of the image was completed.

The user interface presented information on the patient and imaging parameters (Fig. 5b). Additionally, it showed values of the maximal stenosis for each carotid artery (Fig. 5c). Furthermore, the VASIM interface allowed the user to create an overlay of the segmented structures (wall and plaque) using both 2D and 3D lumen models (Fig. 5d).

The bottom panel of the VASIM interface provided a histogram, and image controls, which allowed to change the 2D image stack visualization (Fig. 5e). The right side of the panel D presented a linearized arterial view (Fig. 5d). The panel F (Fig. 5f) provided multiple color maps options, which enabled tissue contrast regulation.

## Discussion

This research aimed to develop a fully-automated tool for the segmentation and analysis of atherosclerosis in the CCA and ICA cervical segments. The main result of the study is a new VASIM software tool. To the authors' knowledge, the VASIM is the first fully-automated, and user-independent tool for carotid arteries CTA images analysis.

In this study, the approaches previously presented by the authors in [6, 9, 12, 16] were revised, improved, and structured. The reliability of the methods mentioned above increased and the computational time for VASIM was reduced.

The new method presented in the study allows skipping the initial and final seed positioning. Unlike in our previous studies, finding two 3D objects in a given volume was unnecessary. This enabled the analysis of images of patients with complete occlusion. Also, the 3D object identification was improved by removing the need to find similar objects bilaterally to the central volume. Contrary to the previous methodology, it was possible to include arteries with loops.

**Table 1** Detailed information about age, sex of patients, localization and morphology of atherosclerotic plaque, and VASIM performance compared with manual stenosis calculation

Patient	Age	Sex	Location of the plaque		Composition of the plaque		Stenosis according to VASIM (%)		Stenosis according to the operator (%)		Absolute difference (%)		Plaque volume (mm <sup>3</sup> )		Time (s)	
			Left	Right	Left	Right	Left	Right	Left	Right	Left	Right	Left	Right	Total	Per slice
1	–	F					0	71					122	94	1211	2.3
2	83	M	ICA	ICA	C, Irr	C, Irr	83	81	79	76	4	5	2879	1229	2286	3.8
3	75	M	ICA	ICA	C	C	0	92	29	75	29	17		0	867	1.9
4	70	M	ICA	ICA	C	C	96	76	19	79	77	3	806	880	381	0.6
5	54	M	ICA		M		0	87	78		78		662	134	0.3	
6	72	F	ICA	ICA	S	M	0	76	90	58	90	18	22	23	787	1.8
7	79	M		ICA		M	100	97		70		27	232	260	426	0.7
8	72	M	ICA	ICA	C	C	34	65	85	73	51	8	0	0	687	2.3
9	73	M														
10	59	M					67	0					707	682	1744	1.8
11	67	F	ICA	ICA	M	C	47	97	69	74	22	23	680	762	2185	2.1
12	34	F					60	89	100		40		185	176	1956	1.7
13	49	F											1063	870		
14	56	M					100	100					274	138	1403	1.5
15	59	F						91		80		11	1085	277	930	0.9
16	78	F												15		
17	50	F					63	89					3926	4048	3133	3.9
18	81	F		ICA		M	71	100	53	72	18	28	272	630	471	0.5
19	78	F	ICA	ICA	C	M			2	36	2	36		261		
20	56	M					0	61					553	651	1977	2.2
21	60	M					0	97					459	1381	588	0.5
22	83	M												8		
23	71	F	ICA	ICA	C	C	99	100	72	74	27	26	2013	1508	948	0.9
24	75	M					65	45							2608	2.9
25	72	M		ICA		C	100	92		16		76	1007	863	785	0.8
26	62	M	CCA	ICA	C	C	96	95		13		82	822	1320	522	0.6
27	77	M	ICA		S		90	100	40		50		395	659	686	0.7
28	72	F					58	0					839	578	2004	2.2
29	12	F					0	0							222	0.5
30	66	F					64	0					1117	926	2126	1.9
31	72	M					52	94						3385	886	0.9
32	69	F	CCA		C		100	86	80		20		620	507	1442	2.9
33	56	M					75	100					44	78	391	0.6
34	69	F														
35	43	F						96						1244	4266	4.6
36	70	F	ICA	ICA	C	C			80	100	80	100				
37	55	M	ICA	ICA	M		95	95	83	77	12	18	183	26	387	0.4
38	77	M						100					1234	1174	699	0.7
39	81	F					84	100					1306	0	305	0.3
40	45	M														
41	66	M	ICA		M		100	100	80		20				604	0.6
42	77	M					87								885	0.8
43	58	F					70	73					245	186	392	0.7
44	37	M											1458	1471		
45	71	M	ICA		M		88	90	80		8		91	93	4630	4.7

**Table 1** (continued)

Patient	Age	Sex	Location of the plaque		Composition of the plaque		Stenosis according to VASIM (%)		Stenosis according to the operator (%)		Absolute difference (%)		Plaque volume (mm <sup>3</sup> )		Time (s)	
			Left	Right	Left	Right	Left	Right	Left	Right	Left	Right	Left	Right	Total	Per slice
46	73	M	ICA		C		99	90	28		71		393	498	0.5	
47	55	M		ICA		U	72	100		42	58	655	565	404	0.4	
48	57	M	ICA		M		81	100	60		21	412	92	553	0.6	
49	47	F					79	0				816	215	231	0.3	
50	77	F					66	81				2088	343	3375	3.5	
51	64	M	ICA	ICA	U	M			44	84	44	84	956			
52	57	F	ICA		M		0	30	100		100			1206	1.3	
53	73	M		ICA			100	61		50	11	4288	543	3911	4.1	
54	54	M					74	68				1072	906	3339	3.3	
55	47	M	ICA	ICA	C	C	0	100	38	63	38	37	143	338	0.4	
56	48	F					87	60						2237	2.6	
57	76	M					0	63				269	835	1510	1.8	
58	75	M	ICA		M		63	85	80		17	1953	2404	2314	2.3	
59	80	F	ICA	ICA	C	C	100	100	72	73	28	27	3296	3917	1807	2.2

Sex: *M* male, *F* female

Location of the plaque: *ICA* internal carotid artery, *ECA* external carotid artery, *CCA* common carotid artery

Composition of the plaque: *M* mixed plaque, *C* calcified lesion, *U* ulcerated lesion, *S* soft lesion, *Irr* irregular plaques

**Table 2** Summary statistics for the stenosis metrics

		Mean	SD
Stenosis	Manual	65%	22 %
	Automatic	74 %	33 %
	Absolute Difference	33%	29%

**Table 3** Data on the number of detected carotid arteries, classified by stenosis level

	<50% stenosis	≥50% stenosis
Manual	11	32
Automatic	19	75

**Table 4** Confusion matrix for stenosis over 50%

		Manual	
		Positive	Negative
VASIM	Positive	25	6
	Negative	5	2

The presented research adopted a more extensive study population (N = 59). The study population enclosed both healthy and diseased patients. The presence of healthy

patients addresses the importance of early diagnosis as a preventive measure. Moreover, the control group enabled for the software adaptation to low stenosis values, allowing analysis among patients with greater differentiation of atherosclerotic lesions. However, higher stenosis levels presented a higher divergence.

In our study, the carotid areas were measured as the perpendicular cross-sections of the lumen to the carotid vessel path. We believe that this gives a more specific indicator than the diameter measured on an individual slice, which is the clinical routine method in the manual analysis. However, this complicates the comparison of the methods, and can partially explain the difference, which is reported in this paper, for manually and automatically calculated stenosis. Other possible reasons are as follows: (i) different locations used for the minimum area and diameter measurements; (ii) the pre-processing of the data before the manual analysis [filtering by radiology workstations and manual improvement performed by an operator (e.g., for partial-volume effect)]; (iii) different measuring vectors used for manual and automatic measurements of the artery diameter.

The algorithm presented in this manuscript is used to assess the severity of atherosclerosis in the CCA and ICA cervical segments, i.e., from the carotid bifurcation until the carotid canal. The anatomical relationship of the ICA to the lateral mass of the atlas (C-1) (the location where ICA is closest to bone tissue) was assessed by Hoh et al.



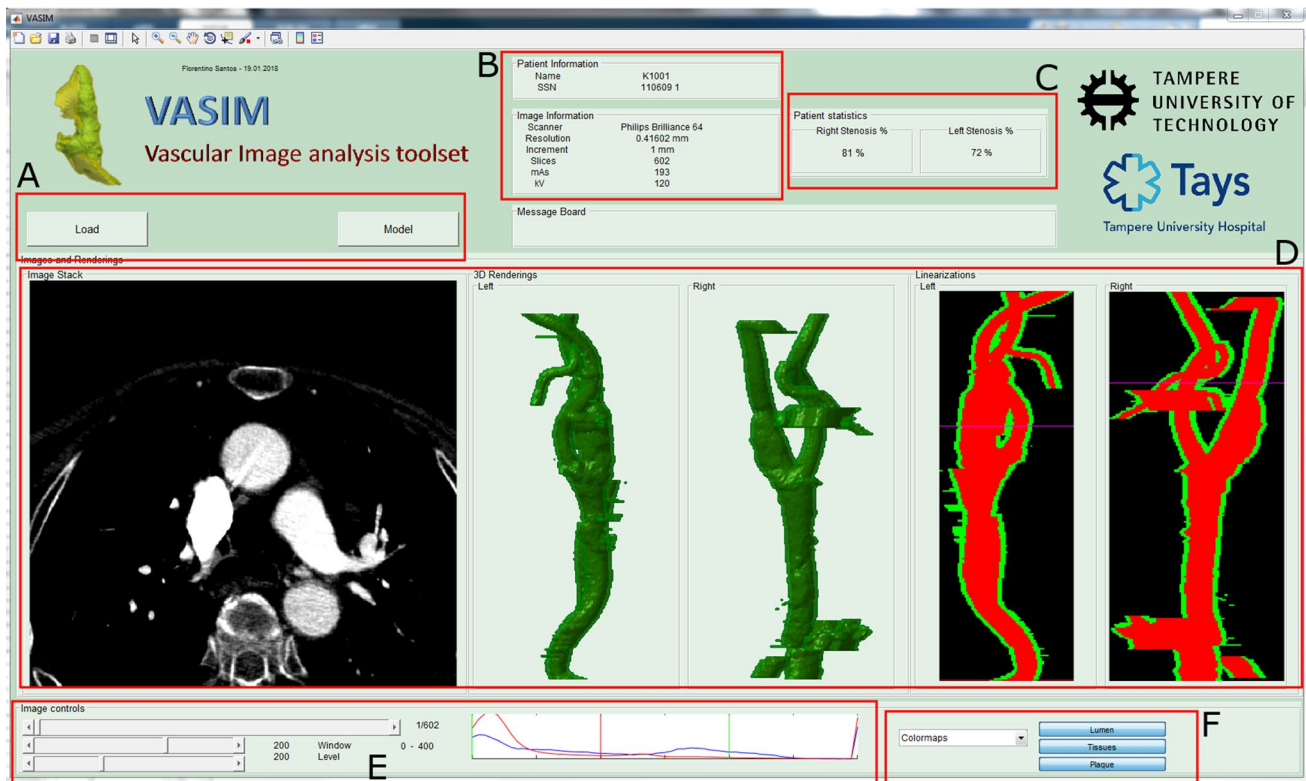


**Fig. 5** VASIM interface (example of Patient 3). **a** VASIM controls. **b** Patient's information. **c** Stenosis level. **d** Patient stack, renderings, and linearizations. **e** Histogram-based window and level controls. **f** Overlay masks' control

[17]. The group studied 100 head-and-neck CT scans. The shortest distance between the ICA and lateral mass of C-1 was 3.5 mm (SD 1.5 mm) and 3.9 mm (SD 1.6 mm) for the left and the right ICA, respectively. The minimum size of a single pixel in CTA scans analyzed by VASIM ranged from 0.4 to 0.7 mm, and maximum slice thickness ranged from 1.0 to 1.25 mm. As the scans were analyzed on pixel-basis, no difficulties in distinguishing vertebrae or foreign objects from the calcified plaque were encountered.

The new metrics reflecting flow dynamics [18–20] and plaque stability may be material for both asymptomatic and symptomatic atherosclerosis patients. To date, all studies in carotid artery flow dynamics area have mainly been performed with magnetic resonance [20–24]. Although the presented study focuses only on CT techniques, the findings may well have a bearing on MRI modalities. In the future, the methods used for analysis of CT images with VASIM could be applied to MRI interpretation, subsequently to adapting the software for that modality. One final possible future application of VASIM is the ability to perform patient follow-up, both for disease progression and after-surgery assessment.

The presented methodology could be expanded to automatically classify plaque composition using attenuation discrimination or texture analysis. The composition is usually

analyzed by evaluating the plaques' components, such as the lipid pool or the calcified cap. Information on the morphology of the plaque is a factor that modulates urgency for surgical treatment. As MRI techniques provide greater soft tissue contrast, adapting VASIM algorithm to this modality would produce better results in the analysis of the plaque composition. Furthermore, because of the more and more pervasive role of artificial intelligence in medicine, VASIM can have a more prominent role in the fusion of image processing and machine learning in medical imaging reporting [25–29]. Such developments can lead not only to full automation of the analysis but also increasing the feasibility of applying such methods in low resource settings, where specialists are less frequent or even inexistent. The fusion of VASIM with artificial intelligence also has potential in the growing field of telemedicine, where it can be applied as a preliminary assessment before operator evaluation.

The presented study was characterized by the following limitations: dependence on the prior stage of the analysis; possible ICA misclassification in case of its total occlusion; manual assessment performed by only one operator; improvable analysis time; unsatisfactory algorithm specificity.

The main study limitation was dependence on the prior stage of the analysis, e.g., if the carotid model was not properly acquired, accurate vascular wall segmentation was impossible.

Moreover, in the case of total stenosis, the correct determination of the segment distant to the occlusion was challenging. It sometimes resulted in misclassification of the ECA's distant section as the ICA.

Another study limitation was the fact, that the manual stenosis degree evaluation was performed by only one trained radiologist, hindering any inter- and intra-operator variability assessment. In addition, we did not have an actual gold standard to check which measurement (manual vs. automatic) was the most accurate. Therefore, the only feasible comparison was between the manually and automatically measured degrees of stenosis.

The average analysis time of 1381 s per patient (1.62 s per slice) remains still long. The carotid path tracking was the most time-consuming step of the analysis. Moreover, the presented methodology involved saving intermediate results, which was critical to the time efficiency. Designing a more efficient algorithm architecture and coding it in a more efficient programming language is crucial. Nevertheless, usually, the radiological analysis of images is not performed in real-time, allowing the VASIM to be run beforehand.

The VASIM algorithm was somehow oversensitive. Although the algorithm sensitivity was 83%, its specificity was only 25%. A possible explanation of the oversensitivity could be the VASIM's tendency to force the segmentation of full arteries. This might cause occluded arteries to be neglected, or misclassification of fibrosis-calcification plaque tissues as the lumen. Notwithstanding these limitations, the overall VASIM accuracy was 71%.

Despite its limitations, the study certainly adds to the rapidly expanding field of automatic CTA image analysis. The aim of the study, i.e., creating a software tool that could be used for carotid arteries automated analysis, with an emphasis on atherosclerosis, was mostly met.

The present research enhanced our previous efforts and produced higher success rates, both in carotid tree 3D volume detection and segmentation (73% vs. 83%) [9]. Besides, this updated version of VASIM was able to detect single carotid arteries, without the need to detect arteries bilaterally [9]. The software was tested in challenging datasets with different tissues and anomalous structures (e.g., plaques, intima-media thickening, and lipid pools) produced by different CT equipment and imaging parameters. Despite improving these areas, there is a need for further development to ensure robustness for use in patients with a wide range of artifacts, clinical and imaging setups, atherosclerotic burden, and anatomy.

## Conclusions

The authors designed and presented the VASIM, a tool for detection, segmentation, and analysis of atherosclerosis in the CCA and the cervical segment of the ICA. The VASIM

is the first comprehensive, fully-automated, and user-independent tool for carotid arteries CTA images analysis.

The VASIM achieved a performance of 83%. The average processing time was 1381 s per patient. The accuracy, sensitivity, and specificity values were 71%, 83%, and 25%, respectively.

The findings from this study contribute in several ways to the field of methods for arterial assessment and provide a basis for the further development of automated atherosclerosis diagnosis and plaque analysis with CTA.

**Acknowledgements** The authors would like to thank Raija Paalavuo RN, Anna-Kaisa Parkkila MD, and Ullamari Hakulinen Lic.Sc., Med. Phys. for their help with patient recruitment and management.

**Author contributions** All authors declare they have contributed to this article. FLCS was responsible for defining the study objectives and design, data collection, development of the image processing and segmentation algorithms, analysis of the data, and statistical analysis. MK was responsible for data collection from the patients files information and stenosis manual calculation. FLCS wrote the manuscript and the co-authors MK, MT, JS, HE, and MP reviewed, commented, and improved the text.

**Funding** FLCS was supported by the CIMO Foundation (Centre for International Mobility; KM-12-8107), Tampere University Hospital, and an iBioMEP doctoral scholarship. MP was supported by the Finnish Cultural Foundation (Central Fund, Grant No. 160735) and by the Academy of Finland (decision number 307967). The project was also partly supported by the Competitive State Research Financing of the Expert Responsibility Area of Tampere University Hospital (Grant No. R07210/9K115).

## Compliance with ethical standards

**Conflict of interest** The authors declare that they have no conflict of interest.

**Ethical approval** All procedures performed in studies involving human participants were in accordance with the ethical standards of the institutional and/or national research committee and with the 1964 Helsinki declaration and its later amendments or comparable ethical standards. This research was approved by the Ethics Committee of the Pirkanmaa Hospital District (decision number R07210).

**Informed consent** Informed consent was obtained from all individual participants included in the study.

## References

1. Beevers DG (2005) The atlas of heart disease and stroke. *J Hum Hypertens* 19(6):505–505
2. Strong K, Mathers C, Bonita R (2007) Preventing stroke: saving lives around the world. *Lancet Neurol* 6(2):182–187
3. Lusis AJ (2000) Atherosclerosis. *Nature* 407:233
4. Enterline DS, Kapoor G (2006) A practical approach to CT angiography of the neck and brain. *Tech Vasc Interv Radiol* 9(4):192–204

5. Vukadinovic D, van Walsum T, Manniesing R, Rozie S, Hameeteman R, de Weert TT, van der Lugt A, Niessen WJ (2010) Segmentation of the outer vessel wall of the common carotid artery in CTA. *IEEE Trans Med Imaging* 29(1):65–76
6. dos Santos FL, Joutsen A, Terada M, Salenius J, Eskola H (2014) A semi-automatic segmentation method for the structural analysis of carotid atherosclerotic plaques by computed tomography angiography. *J Atheroscler Thromb* 21(9):930–940
7. Gates L, Indes J (2014) Evaluation and treatment of carotid artery stenosis. In: Gates L, Indes J (eds) *Carotid artery disease—from bench to bedside and beyond*. IntechOpen, London
8. Markiewicz T, Dziekiewicz M, Maruszyński M, Bogusławska-Walecka R, Kozłowski W (2014) Recognition of atherosclerotic plaques and their extended dimensioning with computerized tomography angiography imaging. *Int J Appl Math Comput Sci* 24(1):33–47
9. Dos Santos FL, Joutsen A, Paci M, Salenius J, Eskola H (2016) Automatic detection of carotid arteries in computed tomography angiography: a proof of concept protocol. *Int J Cardiovasc Imaging* 32(8):1299–1310
10. de Weert TT, de Monye C, Meijering E, Booij R, Niessen WJ, Dippel DW, van der Lugt A (2008) Assessment of atherosclerotic carotid plaque volume with multidetector computed tomography angiography. *Int J Cardiovasc Imaging* 24(7):751–759
11. Ferguson GG, Eliasziw M, Barr HW, Clagett GP, Barnes RW, Wallace MC, Taylor DW, Haynes RB, Finan JW, Hachinski VC et al (1999) The North American symptomatic carotid endarterectomy trial: surgical results in 1415 patients. *Stroke* 30(9):1751–1758
12. Dos Santos FLC, Joutsen A, Salenius J, Eskola H (2014) Fusion of edge enhancing algorithms for atherosclerotic carotid wall contour detection in computed tomography angiography. *Comput Cardiol* 41:925–928
13. Lee TC, Kashyap RL, Chu CN (1994) Building skeleton models via 3-D medial surface axis thinning algorithms. *CVGIP: Gr Models Image Process* 56(6):462–478
14. Otsu N (1979) A threshold selection method from gray-level histograms. *IEEE Trans Syst Man Cybern* 9(1):62–66
15. Aboyans V, Ricco JB, Bartelink MEL, Björck M, Brodmann M, Cohnert T, Collet JP, Czerny M, De Carlo M, Debus S et al (2018) Editor's Choice—2017 ESC guidelines on the diagnosis and treatment of peripheral arterial diseases, in collaboration with the European Society for vascular surgery (ESVS). *Eur J Vasc Endovasc Surg* 55(3):305–368
16. Santos F, Joutsen A, Salenius J, Eskola H (2011) Carotid artery atherosclerosis plaque analysis using ct and histology. In: *Computational vision and medical image processing VIPIMAGE 2011—III ECCOMAS thematic conference on computational vision and medical image processing*, Olhao, Algarve, Portugal, 12–14 October, 2011, CRS Press, Boca Raton pp 1–5
17. Hoh DJ, Maya M, Jung A, Ponrartana S, Laurysen CL (2008) Anatomical relationship of the internal carotid artery to C-1: clinical implications for screw fixation of the atlas. *J Neurosurg Spine* 8(4):335–340
18. Zarins CK, Giddens DP, Bharadvaj BK, Sottiurari VS, Mabon RF, Glagov S (1983) Carotid bifurcation atherosclerosis. Quantitative correlation of plaque localization with flow velocity profiles and wall shear stress. *Circ Res* 53(4):502–514
19. Kwak HS, Yang HJ, Hwang SB, Chung GH (2017) Carotid wall imaging with routine brain MRI to facilitate early detection of carotid plaque and intraplaque hemorrhage. *J Stroke* 19(1):107–108
20. van Hoof RHM, Voo SA, Sluimer JC, Wijnen NJA, Hermeling E, Schreuder F, Truijman MTB, Cleutjens JPM, Daemen M, Daemen JH et al (2017) Vessel wall and adventitial DCE-MRI parameters demonstrate similar correlations with carotid plaque microvasculature on histology. *J Magn Reson Imaging* 46(4):1053–1059
21. Randoux B, Marro B, Koskas F, Duyme M, Sahel M, Zouaoui A, Marsault C (2001) Carotid artery stenosis: prospective comparison of CT, three-dimensional gadolinium-enhanced MR, and conventional angiography. *Radiology* 220(1):179–185
22. Jodas DS, Pereira AS, JM RST (2016) Lumen segmentation in magnetic resonance images of the carotid artery. *Comput Biol Med* 79:233–242
23. Augst AD, Ariff B, Mc GTSA, Xu XY, Hughes AD (2007) Analysis of complex flow and the relationship between blood pressure, wall shear stress, and intima-media thickness in the human carotid artery. *Am J Physiol Heart Circ Physiol* 293(2):H1031–H1037
24. Cheng DC, Billich C, Liu SH, Brunner H, Qiu YC, Shen YL, Brambs HJ, Schmidt-Trucksass A, Schutz UH (2011) Automatic detection of the carotid artery boundary on cross-sectional MR image sequences using a circle model guided dynamic programming. *Biomed Eng Online* 10(1):26
25. Acharya UR, Sree SV, Mookiah MR, Saba L, Gao H, Mallarini G, Suri JS (2013) Computed tomography carotid wall plaque characterization using a combination of discrete wavelet transform and texture features: a pilot study. *Proc Inst Mech Eng H* 227(6):643–654
26. Ambale-Venkatesh B, Yang X, Wu Colin O, Liu K, Hundley WG, McClelland R, Gomes Antoinette S, Folsom Aaron R, Shea S, Guallar E et al (2017) Cardiovascular event prediction by machine learning. *Circ Res* 121(9):1092–1101
27. Menchón-Lara R-M, Sancho-Gómez J-L (2015) Fully automatic segmentation of ultrasound common carotid artery images based on machine learning. *Neurocomputing* 151:161–167
28. Menchón-Lara R-M, Sancho-Gómez J-L, Bueno-Crespo A (2016) Early-stage atherosclerosis detection using deep learning over carotid ultrasound images. *Appl Soft Comput* 49:616–628
29. Nikan S, Gwadry-Sridhar F, Bauer M (2016) Machine learning application to predict the risk of coronary artery atherosclerosis. In: *2016 International conference on computational science and computational intelligence (CSCI)*: 15–17 Dec. 2016, pp 34–39

**Publisher's Note** Springer Nature remains neutral with regard to jurisdictional claims in published maps and institutional affiliations.